Preparation, Characterizations and Theoretical Calculations of a Mg(II) Porphyrin Complex with Axial O-bonded 4-Pyrrolidinopyridine

Souhir Jabli, Bouzid Gassoumi, Soumaya Nasri, H. Ghalla, Emiliano Martìnez-Vollbert, Florian Molton, Frédérique Loiseau, Thierry Roisnel, Habib Nasri

Highlights

- Synthesis of bis(4-pyrrolidinopyridine-κO)[*meso*-tetra(*para*-bromophenyl)porphyrinato)] magnesium(II) (**1**).
- IR, UV-vis, fluorescence, ^{1}H MNR and mass spectroscopy investigations on (**1**).
- Single crystal X-ray molecular structure and Hirshfeld surface analysis of (**1**) are reported.
- Cyclic voltammetry investigation on (**1**).
- DFT, MEP and QTAIM theoretical studies on complex **1**.

Preparation, Characterizations and Theoretical Calculations of a Mg(II) Porphyrin Complex with Axial *O*-bonded 4-Pyrrolidinopyridine

Souhir Jabli [a], Bouzid Gassoumi [b], Soumaya Nasri [a,,c,], H. Ghalla [b], Emiliano Martinez Vollbert [d], Florian Molton [d], Frédérique Loiseau [d], Thierry Roisnel [e], Habib Nasri [a,*]*

[a] : University of Monastir, Laboratory of Physical Chemistry of Materials (LR01ES19), Faculty of Sciences of Monastir, Avenue de l'environnement, 5019 Monastir, Tunisia.
[b]: Laboratory of Advanced Materials and Interfaces (LIMA), University of Monastir, Faculty of Science of Monastir, Avenue of Environment, 5000 Monastir, Tunisia
[c] : Department of Chemistry, College of Science Al-Zulfi, Majmaah University, 11952, Saudi Arabia.
[d]: Département de Chimie Moléculaire, 301 rue de la Chimie, Université Grenoble Alpes, CS 40700, 38058 Grenoble, Cedex 9, France
[e]: Institute of Chemical Sciences of Rennes, UMR 6226, University of Rennes 1, Beaulieu Campus, 35042 Rennes, France.

Abstract

We hereby report the synthesis of a new hexacoordinated magnesium(II) metalloporphyrin with the formula [Mg(TBrPP)(4-pypo-κO)$_2$] (**1**) where TBrPP is the *meso*-tetra(*para*-bromophenyl)porphyrinate and (4-pypo-κO) is the *O*-bonded 4-pyrrolidinopyridine axial ligand. This Mg(II) coordination is considered the linking isomer of the already known *N*-bonded 4-pyrrolidinopyridine (4-pypo-κN) with the formula [Mg(TTP)(4-pypo-κN)$_2$] where TTP is the *meso*-tetra(*p*-tolyl)porphyrinate. Complex **1** was characterized by elemental analysis, IR, ^{1}H NMR, UV/Vis and fluorescence spectrometric techniques, cyclic voltammetry measurements as well as single-crystal X-ray diffraction analysis. The Wingx supported program PLATON and the Hirshfeld surface analysis were both used to elucidate the intermolecular interactions in the crystal lattice of complex **1**.

Computational studies at DFI/B3LYP-D3/6-31G(d,p)-LanL2DZ level of DFT were used to elucidate the minimum energy geometry, the HOMO and LUMO molecular orbitals characteristics and the reactivity of complex **1**. The molecular electrostatic potential (MEP) calculations on complex **1** have been made to determine the electrophilic-nucleophilic character of our new Mg(II) metalloporphyrin. Furthermore, the quantum theory atom in molecule (QTAIM) calculations were performed to get more insights into the type of interactions between the [Mg(TBrPP)] moiety and the two 4-pyrrolidinopyridine axial ligands of complex **1**.

* Corresponding authors:
E-mail address: hnasri1@gmail.com (Habib Nasri) and soumaya.n@mu.edu.sa (S. Nasri)

Keywords: Magnesium(II) porphyrin complex; X-ray molecular structure; Cyclic voltammetry; DFT, MEP and QTAIM calculations.

1. Introduction

For many decades, porphyrins have been the subject of intense research in numerous areas such as artificial photosynthesis, molecular electronic devices, electrochemical sensors and electrocatalysis.
Since the sixteens, porphyrin complexes with open-shell paramagnetic d transition metal ions such as Fe(II), Fe(III), Co(II) and Mn(III) have been extensively studied as they serve especially as biomimetic models for hemoproteins **[1]**. Diamagnetic metalloporphyrins with the divalent metals Zn(II), Cd(II) and Mg(II) were also studied since the seventies, especially those with Zn^{2+} as the center ion. Notably the center metals of porphyrin complexes with zinc, cadmium and magnesium are unambiguously in the +2 oxidation state. This makes these diamagnetic species ideal for studying the effect of the axial coordination of ligands without worrying about the change of the oxidation state of the center metal during the reaction for instance which is not the case with open-shell paramagnetic d transition metal ions such as Fe^{3+}, Co^{2+} and Mn^{3+}. During the last fifteen years, we and other research groups reported many investigations on Mg(II) metalloporphyrins **[2-6]**. These magnesium(II) porphyrinic species are known to exhibit higher fluorescence quantum yields and longer excited state lifetimes compared to those of other metalloporphyrins such as Zn(II) porphyrin complexes **[7]**. Mg(II) porphyrins have been tested in many areas such as catalysis **[8-12]**, sensors **[13,14]** and environmental applications **[15,16]**.
It is also noteworthy that all known structures of cadmium(II) porphyrin complexes are pentacoordinate because of the large size of the Cd^{2+} ion which cannot fit the size of a porphyrin macrocycle.
An inspection of the Cambridge Structural Database (CSD Version 5.43, last update September 2022) **[17]** shows that magnesium(II) porphyrin complexes can be pentacoordinated or hexacoordinated. In the case where the axial ligand X is anionic such as N_3^- and SCN^- the corresponding metalloporphyrin is in all cases pentacoordinate type [Mg(Porph)X]- (Porph = porphyrinate). This is not the case if the axial ligand L is a neutral *N*-donor or *O*-donor where we can have either a pentacoordinated complex of type [Mg(Porph)(L)] or a hexacoordinated coordination compound type $[Mg(Porph)(L)_2]$. Predicting the

coordination polyhedron of the central metal Mg^{2+} for a given porphyrin and a given neutral axial ligand L is not so straightforward. Indeed, in the case where the axial ligand is H_2O, with TPP (*meso*-tetraphenylporphyrinate) one expects to obtain the hexacoordinated complex [Mg(TPP)(H_2O)$_2$] whereas with TBrPP (*meso*-tetra(*para*-chlorophenyl)porphyrinate), one expects to obtain the pentacoordinated complex [Mg(TBrPP)(H_2O)] since for the two *meso*-arylporphyrins, H atom (for TPP) is less donor than the Br atom (for TBrPP). However, in the solid state, the complexes [Mg(TPP)(H_2O)] **[18]** and [Mg(TBrPP)(H_2O)$_2$] **[19]** are obtained. In a previous paper **[4]** we reported the preparation, the spectroscopic, electrochemical and the structural of the 4-pyrrolidinopyridine Mg(II) *meso*-tetratolylporphyrin with the formula [Mg(TTP)(4-pypo-κN)$_2$] (TTP = *meso*-tetratolylporphyrin, 4-pypo-κN = *N*-coordinated 4-pyrrolidinopyridine) (Scheme 1).

In order to get more insights into the chemistry of magnesium(II) porphyrin compounds, their coordination type with neutral ligands as well as their spectroscopic, electrochemical properties, a new hexacoordinated bis(4-pyrrolidinopyridine-*O*)[*meso*-tetra(*para*-bromophenyl)porphyrinato)]magnesium(II) porphyrin with the formula [Mg(TBrPP)(4- pypo-κO)$_2$] (**1**) (4-pypo-O = 4-pyrrolidinopyridine-*O*) is investigated.

This new Mg(II) *meso*-arylporphyrin complex could be considered the linking isomer of the [Mg(TTP)(4-pypo-κN)$_2$] **[4]** for which the 4-pyrrolidinopyridine axial ligand is *N*-bonded to Mg(II) while in our new [Mg(TBrPP)(4-pypo-κO)$_2$] (**1**) the 4-pyrrolidinopyridine ligand is *O*-bonded to Mg(II) (Scheme 1).

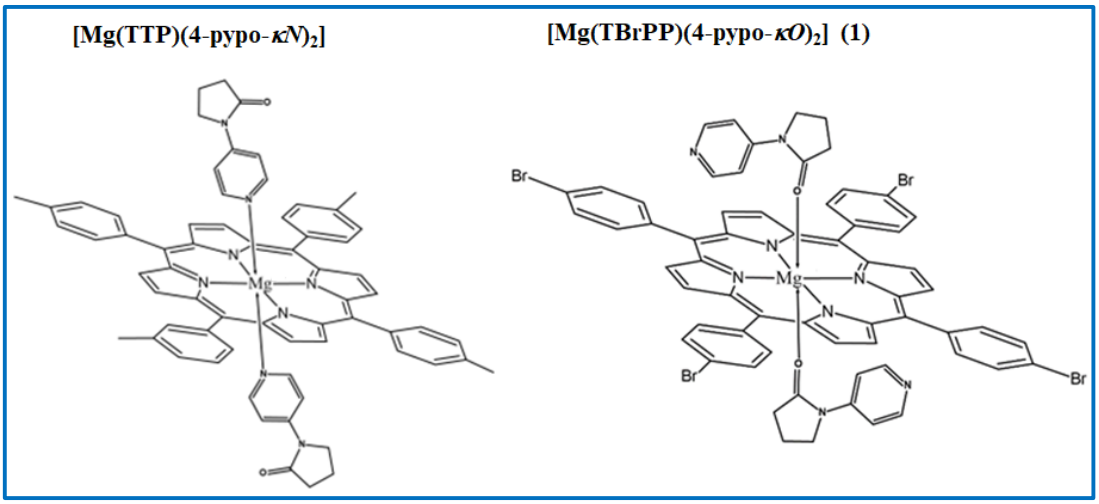

Scheme 1. Schematic representations of [Mg(TTP)(4-pypo-κN)$_2$] **[4]** and [Mg(TBrPP)(4-pypo-κO)$_2$] (**1**).

Furthermore, the DFT, MEP calculations, the Topological Quantum Theory of Atoms in Molecules (QTAIM) and the Non-Covalent Interactions - Reduced Density Gradient (NCI-RDG) analyses were performed on complex **1** to better understand the reactivity of this new Mg(II) porphyrin species and investigate the interactions between the [Mg(TBrPP)] moiety and the two 4-pyrrolidinopyridine axial ligands.

2. Experimental Section

2.1. Materials and methods

IR and UV-vis spectroscopy: Solid IR spectra were obtained with a PerkinElmer Spectrum Two FTIR spectrometer. The UV/Vis spectra were recorded with a WinASPECT PLUS (validation for SPECORD PLUS version 4.2) scanning spectrophotometer.

MS spectrometry: Electrospray (ESI) spectra were carried out using an amaZon speed ion trap instrument and the ESI-HRMS spectra were recorded using the LTQ Orbitrap XL apparatus (Thermo Scientific) equipped with an electrospray ionization (ESI) source. Dichloromethane solutions were used for the analysis.

Emission spectroscopy: The emission spectra were recorded at room temperature with a Horiba Scientific Fluoromax-4 spectrofluorometer. The luminescence lifetime measurements were performed for excitation at $\lambda = 450$ nm using the second harmonic of a titanium–sapphire laser (picosecond Tsunami laser spectra physics 3950-M1BB and 39868-03 pulse picker doubler) at an 800 kHz repetition rate. Fluotime 200 from AMS technologies was used for the decay acquisition. It consists of a GaAs microchannel plate photomultiplier tube (Hamamatsu model R3809U-50) followed by a time-correlated single photon counting system from Picoquant (PicoHarp300). The ultimate time resolution of the system is close to 30 ps. The luminescence decays were analysed with the FLUOFIT software available from Picoquant. The mission quantum yields were determined at room temperature in dichloromethane solutions by using the optically dilute method. [Zn(TPP)] in an air-equilibrated dichloromethane solution was used as a quantum yield standard ($\phi_f = 0.031$) **[20]**.

Electrochemistry: Cyclic voltammetry (CV) experiments were performed with ~~a~~ CH-660B potentiostat (CH Instruments). All analytical experiments were conducted at room temperature under an argon atmosphere (argon stream) in a standard one compartment, three-electrode electrochemical cell. Tetra-*n*-butylammonium perchlorate (TBAP) was used as a supporting electrolyte (0.2 M) in dichloromethane

previously distilled over calcium hydride under argon. An automatic ohmic drop compensation procedure was systematically implemented before the CV data were recorded with electrolytic solutions containing the studied compounds at concentrations of ca. 10^{-3} M. CH Instruments vitreous carbon (ϕ = 3 mm) working electrodes were polished with 1 mm diamond paste before each recording. The $Ag/AgNO_3$ 0.01 M (TBAP 0.2 in CH_2Cl_2) redox couple was used as the reference electrode. The potential of the ferrocene/ferrocenium redox couple was used as an internal reference (86 mV vs. $Ag/AgNO_3$ under our experimental conditions). For comparison with previously published data, all potentials given in the text and in Table 5 have been converted to values relative to the saturated calomel electrode (SCE) according to the following relationship: $E(SCE) = E(Ag/AgNO_3) + 298$ mV.

2.2. Synthesis

2.2.1. Synthesis of [Mg(TBrPP)]

Solvents were appropriately distilled and dried before use and the reagents employed were commercially available and were used as received without further purification. The *meso*-tetra(*para*-bromophenyl)porphyrin (H_2TBrPP) and the Mg(II)-metallated porphyrin [Mg(TBrPP)] starting materials were prepared as described in the literature **[21,22]**. The ^{1}H NMR spectra of H_2TBrPP and [Mg(TBrPP)] starting materials are reported in the supplementary information (Figures S3 and S4).

2.2.2. Synthesis of [Mg(TBrPP)(4-pypo-*κO*)$_2$] (1)

[Mg(TBrPP)] (30 mg, 0.031 mmol) and 4-pyrrolidinopyridine (90 mg, 0.608 mmol) were dissolved in 5 mL of dichloromethane and stirred at room temperature overnight. The color of the solution changed to green blue. The obtained compound crystallizes by slow diffusion of *n*-hexane through the dichloromethane solution to give dark-blue crystals (40 mg, 82 %) after one week.

Elemental analysis calcd (%) for $C_{62}H_{46}Br_4MgN_8O_2$, C 58.22, H 3.63, N 8.76; found: C 59.61, H 3.88, N 8.79; (ESI) (dichloromethane): *m*/*z* $[Mg(TBrPP)(L)_2]^+$ (L = 4-pypo, $C_9H_{10}N_2O$) calcd for $C_{62}H_{46}Br_4MgN_8O_2$: 1274.03; found 1277.09; UV–vis: λ_{max} (nm) in CH_2Cl_2: 427, 564, 604; FT-IR [solid neat, $\bar{\nu}$ (cm^{-1})]: ν[CH Porph] 2970–3024, ν[ν(C=C) and [ν(C=N) porph)] 1583 cm^{-1}; [ν(C=C) and [ν(C=N) O-pypo)]1692, [ν(C=O) O-pypo ligand] 1719-1745 cm^{-1}; ^{1}H NMR (300 MHz, $CDCl_3$ δ (ppm): 8.84 (Hβ-pyrrol), 8.05 ($H_{o,o}$ Porph), 7.86 ($H_{m,m'}$ Porph), 7.92 (H_L O-pypo), 7.12($H_{L'}$ O-pypo), 2.44 (H_g O-pypo), 3.68 (H_e O-pypo) and 2.06 (H_f O-pypo).

2.3. X-ray structure determination

A dark blue single crystal of dimensions 0.40 x 0.20 x 0.12 mm of complex (**1**) was chosen for an X-ray diffraction study. Crystal evaluation and data collection were performed on a Bruker-AXS-Enraf-Nonius Kappa APEXII diffractometer equipped with a CCD area detector with Mo Kα radiation of wavelength (λ = 0.71073 Å) at 200(2) K during data collection. The data were scaled and corrected for absorption correction using SADABS-2004/1 (Bruker, 2004) **[23,24]** and refined by full-matrix least-squares techniques based on F^2 by using the SHELXL-2014 program **[25]**. All non-hydrogen atoms were refined with anisotropic atomic displacement parameters. C-bound hydrogen atoms were included in geometrically calculated positions and N-bound hydrogen atoms were initially located from a difference Fourier map and subsequently included using a riding model. Drawings were made using ORTEP3 for windows **[26]** and MERCURY **[27]** correction using SADABS-2004/1 (Bruker, 2004) **[23]**. The structure was solved by direct methods by using SIR-2014 **[24]** and refined by full-matrix least-squares techniques on F^2 by using the SHELXL-2014 program **[25]**. All non-hydrogen atoms were refined with anisotropic atomic displacement parameters. C-bound hydrogen atoms were included in geometrically calculated positions and N-bound hydrogen atoms were initially located from a difference Fourier map and subsequently included using a riding model. Drawings were made using ORTEP3 for Windows **[26]** and Mercury **[27]**. The crystallographic data and structural refinement details of **1** are shown in Table 1. Selected bond lengths and angles for this compound are listed in Table 2.

Table 1. Crystal data and structural refinement for [Mg(TBrPP)(4-pypo-κO)$_2$] (**1**).

Formula	$C_{62}H_{44}Br_4MgN_8O_2$
M.W.	1277.01
Crystal System	triclinic
Crystal	*P-1*
a (Å)	9.5600 (19)
b (Å)	11.746 (2)
c (Å)	12.911 (3)
α (°)	87.45 (3)
β (°)	70.06 (3)
γ (°)	79.44 (3)
V (Å^3)	1339.6 (6)
Z	1
$\rho_{calc.}$/ g.cm^{-3}	1.583
μ/ mm^{-1}	3.070

F(000)	640
Crystal size (mm^3)	0.40 x 0.20 x 0.12
Crystal Color	violet
Crystal Shape	block
T(K)	150 (2)
θ_{min} - θ_{max} (°)	2.303– 26.000
Limiting indices	-11 ≤ h ≤ 11, -14 ≤ k ≤ 14, -15 ≤ l ≤ 15
R(int)	0.0620
Total/Unique data	26067/5095
Observed data [$I_o > 2\sigma(F_o)$]	4025
Parameters	349
S [Goodness of fit]	1.123
R_1[a], wR_2[b] [$F_o > 4\sigma(F_o)$]	R_1 = 0.0578, wR_2 = 0.1421
wR_2[b] [all data]	R_1 = 0.0795, wR_2 = 0.1585
CCDC	2220695

[a] :$R1 = \Sigma||F_O|-|F_C||/\Sigma|F_O|$, [b] :$wR2 = \{\Sigma[w(|F_O|^2-|F_C|^2)^2]/\Sigma[w(|F_O|^2)^2]\}^{1/2}$.

Table 2. Selected bond lengths (Å) and angles (°) of complex **I**.

Magnesium coordination polyhedron			
Mg-N1	2.071(4)	N2-Mg-N1	90.98(14)
Mg-N2	2.071(4)	N2-Mg-O1	94.50(15)
Mg-O1	2.223(4)	N1-Mg-O1	89.83(15)
4-pyrrolidinopyridine *(4-pypo-κO) Axial ligand*			
O1-C23	1.224(6)		
N3-C23	1.364(7)	N4-C29	1.330(8)
N3-C26	1.466(7)	N4-C30	1.329(8)
O1-C23-N3	125.3(5)	C23-N3-C27	124.7(4)
O1-C23-C24	126.8(5)	C23-N3-C26	113.4(4)
N3-C23-C24	107.9(5)	C30-N4-C29	115.6(5)

3. Results and Discussion

3.1. Synthesis of [Mg(TBrPP)(4-pypo-κO)$_2$] (1)

The bis(4-pyrrolidinopyridine-κ*O*)[*meso*-tetra(*para*-bromophenyl)porphyrinato]magnesium(II) complex with the formula [Mg(TBrPP)(4-pypo-κ*O*)$_2$] (**1**) was prepared by the same protocol than that used to prepare what we are going to refer to as the linkage isomer [Mg(TTP)(4-pypo-κ*N*)$_2$] **[4]** by

reacting the [Mg(TBrPP)] starting material with an excess of 4-pyrrolidinopyridine in dichloromethane at room temperature (Scheme 2).

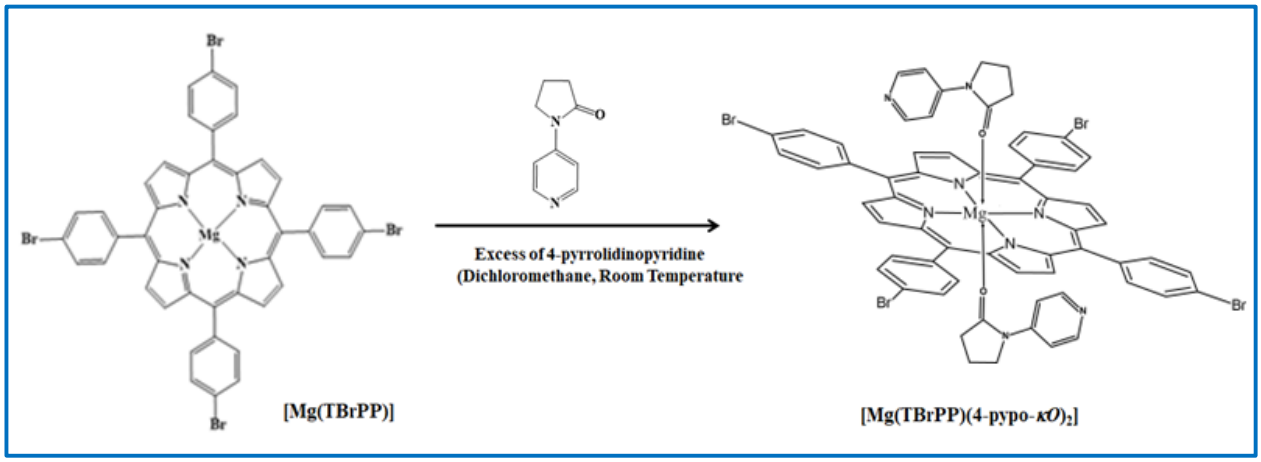

Scheme 2. Synthetic scheme of [Mg(TBrPP)(4-pypo-κO)$_2$] (**1**).

As shown by the X-ray molecular structure (see crystallographic section 3.4), for complex **1**, the two 4-pyrrolidinopyridine axial ligands are coordinated to the Mg^{2+} center ion through the oxygen atom and not through the nitrogen atom of the pyridyl group of the 4-pyrrolidinopyridine. Therefore, complex **1** with the formula [Mg(TBrPP)(4-pypo-κO)$_2$] could be considered the linking isomer of the already reported [Mg(TTP)(4-pypo-κN)$_2$] complex **[4]** even though in both "isomers" we have different porphyrinates (TBrPP and TPP, respectively).

The preference of O-binding in Mg(TBrPP)(4-pypo-κO)$_2$] (**1**) over N-binding in [[Mg(TTP)(4-pypo-κN)$_2$] is straightforward. The four electron-withdrawing *para*-bromo groups of the (4-pypo-κO) isomer (**1**) makes the Mg^{2+} center relatively harder compared to the four electron-donating *para* methyl groups of the (4-pypo-κN) linking isomer.

The subtle change in the electronic properties of the porphyrin ligand is probably responsible for the linkage isomerism. This is confirmed by the cyclic voltammetry data for these two isomers (see cyclic voltammetry section).

3.2. Mass spectrometry, IR and ^{1}H NMR spectroscopies

The electrospray ionization (ESI) mass spectrum of complex **1** depicted in Figure 1 shows the presence of the $[Mg(TTP)(4\text{-pypo-}\kappa O)_2+5H]^{5+}$ fragment. This is an indication of the existence of the bis(4-pypo-κO)-Mg(II)-TCPP (**1**) species in solution.

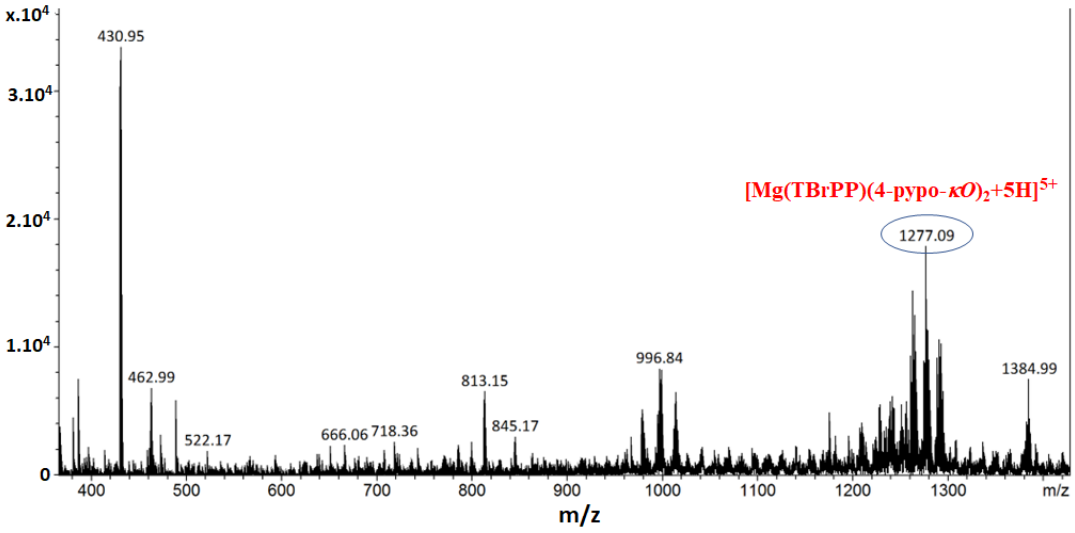

Figure 1. ESI spectrum of $[Mg(TTP)(4\text{-pypo-}\kappa O)_2]$ (**1**), recorded in dichloromethane with a concentration of 5.10^{-3} M.

The IR spectra of the H_2TBrPP free base porphyrin and the [Mg(TBrPP)] starting material are depicted in Figures S1 and S2 while the IR spectrum of complex **1** is illustrated in Figure 2. The absorption bands corresponding to the ν(CH) stretching frequency of H_2TBrPP and [Mg(TBrPP)] are shown between 2970 and 2840 cm^{-1} while the deformation frequency δ(CCH) of the *meso*-arylporphyrin moiety appears at 966 and 1002 cm^{-1} for H_2TBrPP and the metalated porphyrin, respectively **[28]**. The absorption bands of complex **1** shown between 3090 and 2881 cm^{-1} are attributed to the ν(CH) stretching vibration of both TBrPP porphyrinate and the 4-pypo-κO axial ligand. The presence of this axial ligand is confirmed by a strong absorption band at 1690 cm^{-1} attributed to the ν(C=O) stretching of the carbonyl group of this ligand.

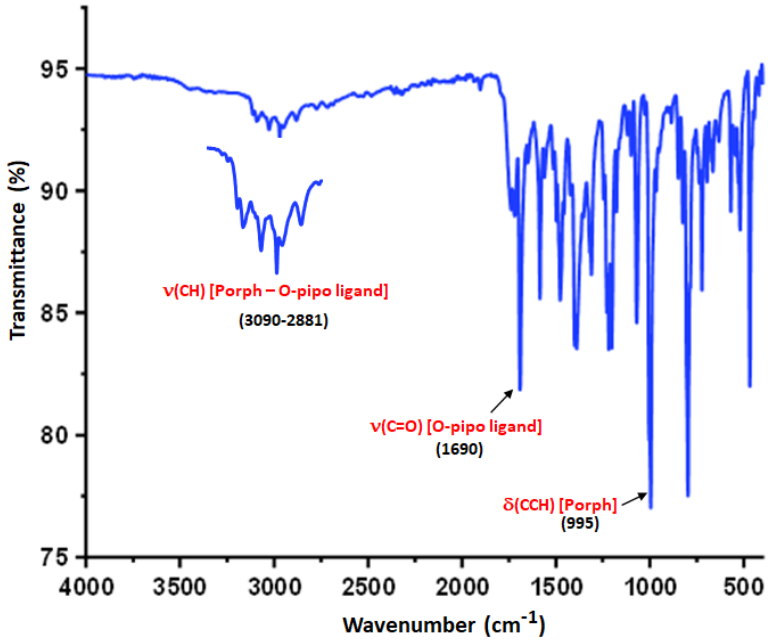

Figure 2. Neat IR spectrum of [Mg(TBrPP)(4-pypo-κO)$_2$] (**1**).

The ^{1}H NMR spectra of H_2TBrPP and the [Mg(TBrPP)] starting material are shown in Figures S3 and S4 which are characteristic of *meso*-arylporphyrin species. Our new Mg(II) hexacoordinated porphyrin coordination compound (**1**) exhibits a ^{1}H NMR spectrum very similar to that of the [Mg(TPP)(4-pypo-κN)$_2$] **[4]** (Figure 3) related compound in which the 4-pyrrolidinopyridine ligand is coordinated to the Mg center metal through the nitrogen atom of the pyridyl group of the axial ligand. Thus, the H_L, $H_{L'}$, H_e, H_g and H_f protons of the 4-pyrrolidinopyridine of both two coordination compounds present chemical shifts very close (Table 3) indicating that the N/O coordinating mode does not affect the HMR resonance of these two linking isomers.

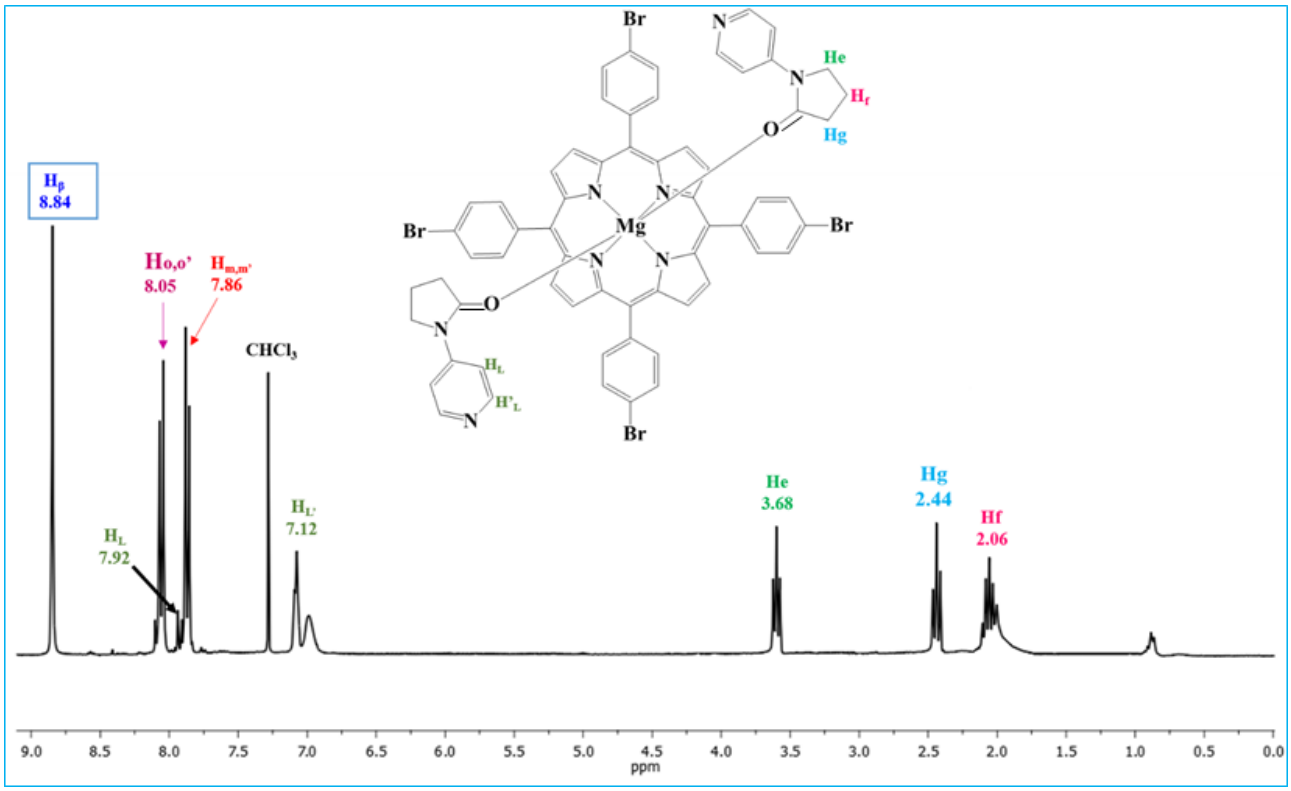

Figure 3. ^{1}H NMR spectrum of [Mg(TBrPP)(4-pypo-κO)$_2$] (1) recorded in $CDCl_3$ at room temperature with concentration C ~10^{-3} M.

Table 3. Chemical shift values complex **1** and [Mg(TTP) (4-pypo-κN)$_2$].

Complex	Hβ-pyrrolic	H-phenyl	HL/HL'	He/Hg/Hf	Ref.
[Mg(TTP)(4-pypo-κN)$_2$]	8.84	8.06, 7.33	8.06/7.50	3.68/2.52/2.09	**[4]**
[Mg(TBrPP)(4-pypo-κO)$_2$]	8.84	8.05, 7.33	7.82/7.12	3.68/2.44/2.06	t.w.

3.3. Photophysical properties

The UV/Vis spectrum of **1** (Figure 4) presents a strong B band, known as the Soret band, corresponding to the $S_o \leftarrow S_2$ transition centered at 427 nm and two weaker absorption bands [Q(1,0) and Q(0,0)] corresponding to the $S_o \leftarrow S_1$ transition with values of 565 and 604, respectively. These values are practically the same as those of the [Mg(TTP)(4-pypo-κN)$_2$] linking isomer **[4]**.

In the same Figure 4 is shown the fluorescence spectrum of **1** for which the fluorescence bands Q(1,0) and Q(0,0) correspond to the $S_o \leftarrow S_1$ transition. The λ_{max} values of these bands are 610 nm and 655 nm, respectively. These values are also practically the same as those of the [Mg(TTP)(4-pypo-κN)$_2$] linking isomer.

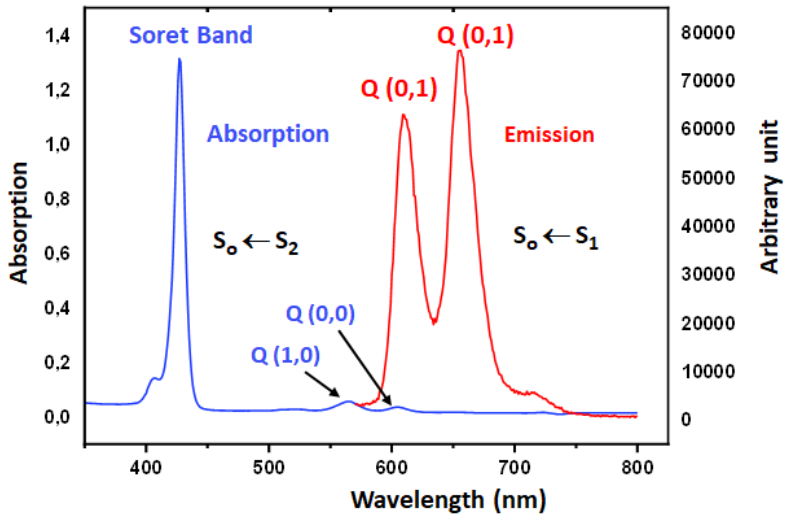

Figure 4. UV/Vis spectrum (in blue) and fluorescence spectrum (in red) of complex **1**. The spectra were recorded at room temperature in dichloromethane with concentrations ~ 10^{-6} M.

The energy (in nm) and the electronic transitions of the [Mg(TBrPP)(4-pypo-κO)$_2$] (**1**) complex were calculated at the B3LYP/GENECP level of theory from the theoretical absorption spectrum. The UV/vis absorption spectrum of complex **1** in dichloromethane solution is displayed in Figure 5. The theoretical Soret band is observed at 414 nm while the theoretical Q band is centred at 578 nm. These values are considered close to the experimental values of the Soret and the Q(0,1) bands (compared to 427 and 565 nm, respectively). A zoom performed by the software on the Q band (Figure 5-b), gives only a second theoretical absorption band located at 582 nm, which is experimentally visualized at 604 nm.

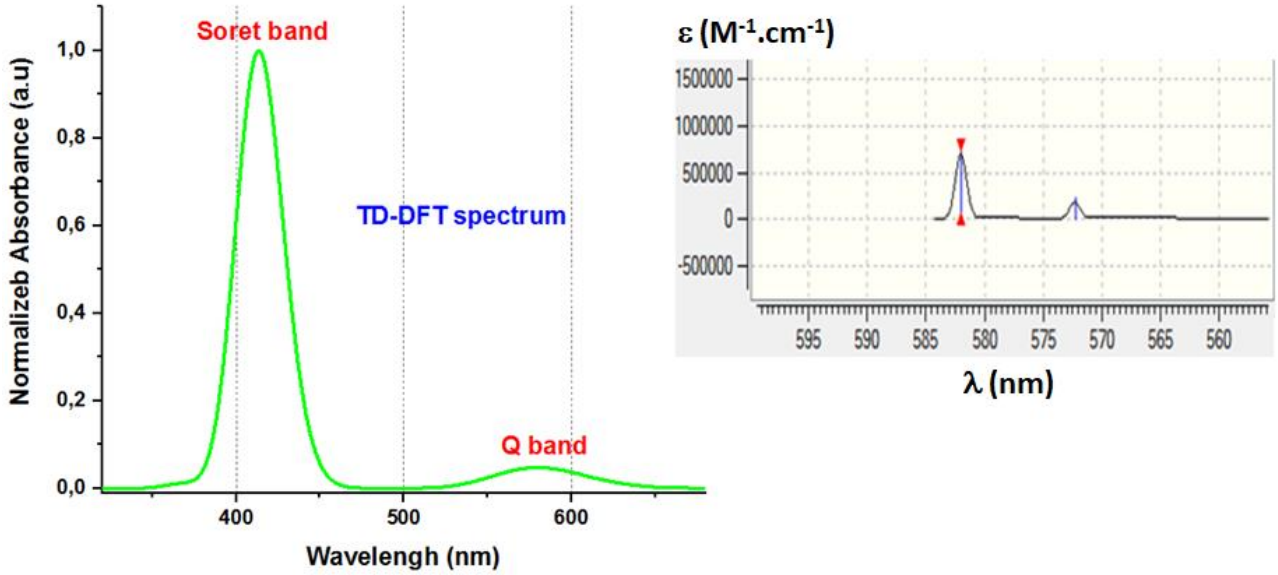

Figure 5. Theoretical UV/Vis spectrum complex **1**. **(a):** full-range spectrum, **(b):** Spectrum enlargement in Q band region.

We determined the experimental optical energy gap ($E_{g\text{-}obt}$) of complex **1** from the $(\alpha h\nu)^2$ versus the photon energy ($E = h\nu$) **[29]** where α is the absorption coefficient, h is the Planck constant and *v* is the frequency ($\nu = 1/\lambda$) (Figure S5). The $E_{g\text{-}opt}$ energy value is 2.247 eV which is an indication that our Mg-TBrPP-(4-pypo-*κO*) derivative is considered a semi-conductor. On the other hand, the calculated energy gap is found to be equal to 2.55 eV.

As a conclusion of this photophysical study on complex **1**, it can be said that the electronic properties of magnesium(II) complexes with *meso*-porphyrins do not depend on either the *para*-substituted groups in the phenyl positions of the *meso*-porphyrins or on the type of the axial ligand.

3.4. X-ray Molecular Structure of [Mg(TBrPP)(4-pypo-*κO*)$_2$]

Complex **1** crystallized in the triclinic crystal system with a *P-1* space group and one formula per unit cell (Z = 1). The asymmetric unit of **1** is made by one half [Mg(TBrPP)(4-pypo-*κO*)$_2$] coordination compound. In Figure 6 is illustrated the Ortep view of this new magnesium(II) metalloporphyrin.

An inspection of Table 4 shows that pentacoordinate magnesium(II) *meso*-arylporphyrins present values of the mean plan equatorial distance between the center metal Mg(II) and the nitrogen atoms of pyrrole rings (Mg—Np) ranging between 2.082 and 2.110 Å. These distances are longer than those of hexacoordinate Mg(II) metalloporphyrins which are ~ 2.070 Å. This is the case of [Mg(TBrPP)(4-pypo-κO)$_2$] (**1**) with a Mg—Np = 2.071(4) Å. The Mg—O(4-pypo-κO) bond length of complex **1** is 2.223(4) Å which is close to that of the hexacoordinate biaqua species [Mg(TBrPP)(H$_2$O)$_2$] **[19]** with a Mg—O(H$_2$O) distance of 2.221 Å.

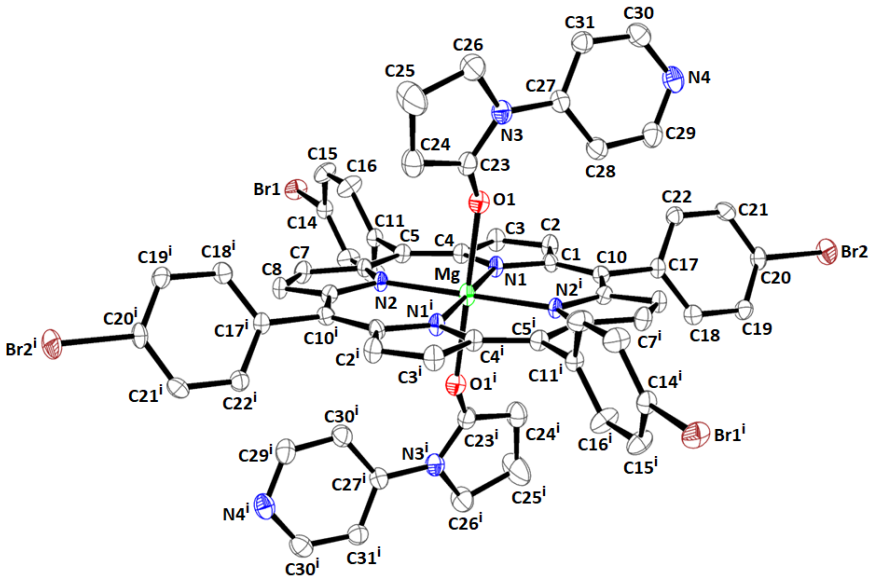

Figure 6. Ortep diagram of [Mg(TBrPP)(4-pypo-κO)$_2$] (**1**).

The two 4-pypo-κO *trans* axial ligands are parallel and bisect two neighboring pyrrole rings as is the case of the majority of metalloporphyrins and hemoproteins (Figure 7-a). Both Figures 7-a and 7-b show that the two *para*-bromophenyl rings close to the two 4-pypo-κO axial ligands are tilted away from their normal positions, i.e., nearly perpendicular to the plan of the porphyrin core. Thereby, we get a minimum interaction between the 4-pypo-κO axial ligands and these two phenyl groups.

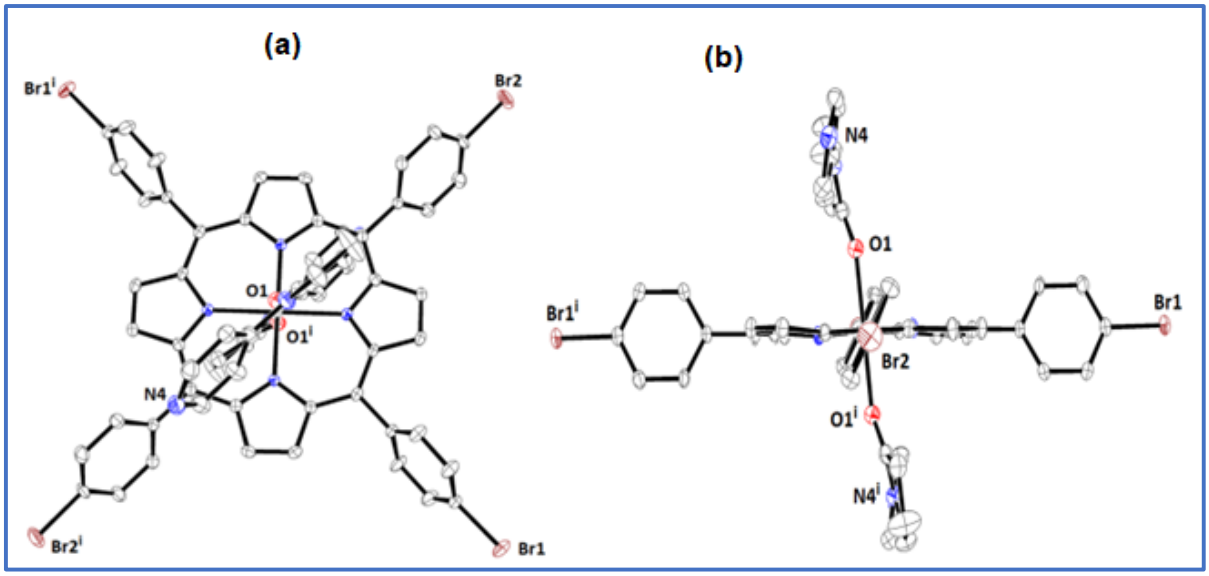

Figure 7. Ortep views showing the orientation of the two 4-pyrrolidinopyridine axial ligands.

Table 4. Selected bond lengths [Å] and angles [°] for [Mg(TBrPP)(4-pypo-κO)$_2$] (**1**) and a selection of several related Mg(II) *meso*-arylporphyrins.

Complex	Mg__N_p[a]	Mg–X_L[b]	Ref.
Pentacoordinated magnesium(II) meso-porphyrins			
[Mg(TPP)(H_2O)][c]	**2.092(7)**	2.012 (6)	**[30]**
[Mg(TBrPP)(4,4-bpy)][d]	**2.090(3)**	2.143(5)	**[31]**
[Mg(TClPP)(DMAP)][e,f]	**2.082(3)**	2.130 (4)	**[6]**
[Mg(TBrPP)(HIm)][g]	**2.094(2)**	2.120 (3)	**[2]**
[K(222)][Mg(TPP)(NCO)][c,i]	**2.110**	2.047	**[3]**
Hexacoordinated magnesium(II) meso-porphyrins			
[Mg(TPP)(pipz)$_2$][c,j]	**2.073**	2.423	**[32]**
[Mg(TPP)(py)$_2$][c,k]	**2.072**	2.376	**[33]**
[Mg(TBrPP)(pyz)$_2$][l]	**2.070(3)**	2.350(4)	**[31]**
[Mg(TPP)(1-MeIm)$_2$][c,m]	**2.071(6)**	2.297(8)	**[32]**
][Mg(TPP)(H_2O)$_2$].(18-C-6)[c,n]	**2.071**	2.213	**[34]**
[Mg(TBrPP)(H_2O)$_2$]	**2.069**	2.221	**[19]**

[Mg(TPP)(4-Mepy)$_2$][c,o]	**2.070**	2.385	**[32]**
[Mg(TTP)(4-pypo-κN)$_2$][p]	**2.070(3)*** **2.076(3)****	2.310(3)/2.292(3)* 2.302(3)**	**[4]**
[Mg(TBrPP)(4-pypo-κO)$_2$] (**1**)	**2.071(4)**	2.223(4)	t.w.

[a]: M—N_p = average equatorial Mg-nitrogen pyrrole rings distance, [b]: Mg—X_L = center metal Mg-axial ligand distance, [c]: TPP = *meso*-tetraphenylporphyrinate, [d]: 4,4'-bpy = 4,4'-bipyridine, [e]: TClPP = *meso*-tetrakis(*para*-chlorophenyl)porphyrinate, [f]: DMAP = 4-dimethylaminopyridine, [g]: HIm = imidazole, [i]: 222 = cryptand-222, [j]: pipz = piperazine, [k]: py = pyridine, [l]: pyz = pyrazine, [m]: 1-MeIm = 1-Methylimidazole, [n]: 18-C-6: 18-crown-6, [o]: 4-Mepy = 4-Methylpyridine N-oxide, [p]: TTP = *meso*-tetra(*p*-tolyl)porphyrinate, *: for the full molecule 1, **: for the half molecule 2.

We notice that in both two [Mg(TBrPP)(4-pypo-κO)$_2$] and [Mg(TPP)(4-pypo-κO)$_2$] linking isomers, the two 4-pyrrolidinopyridine axial ligands are parallel.

As illustrated in Figure 8, the crystal packing of **1** presents small voids (~1% of the unit cell and a volume of ~13 Å^3) parallel to the [100] direction located between [Mg(TBrPP)(4-pypo-κO)$_2$] molecules.

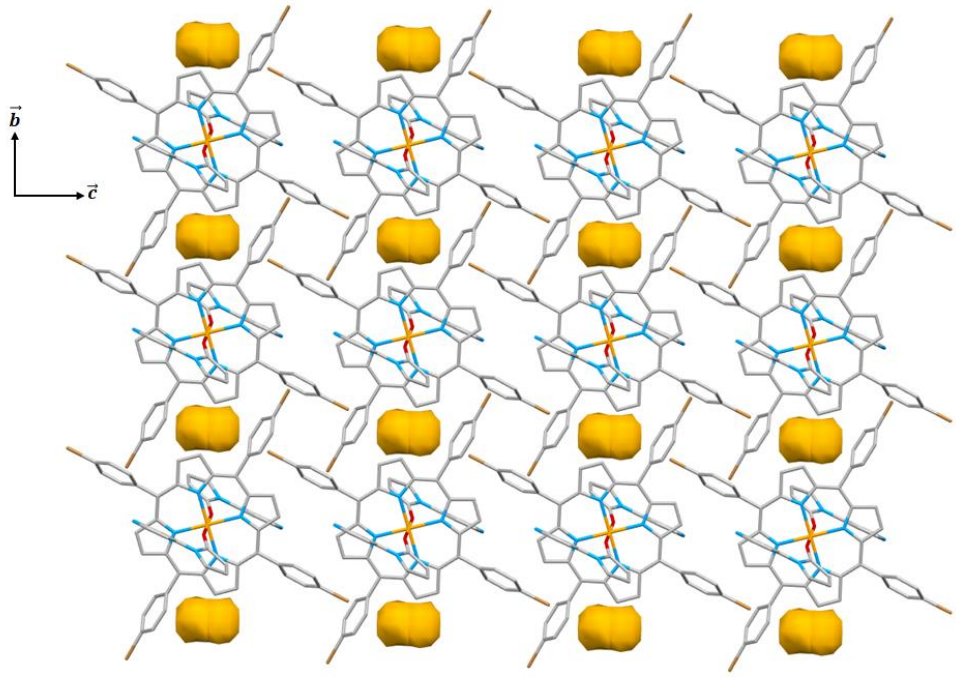

Figure 8. Packing diagram of complex **1** showing voids down the *a* axis. A ball radius of 1.2 Å and a grid of 0.7 Å were used to calculate the voids.

In the crystal lattice of **1**, two [Mg(TBrPP)(4-pypo-κO)$_2$] molecules are linked together by weak π-π interactions involving Cg···Cg interactions between the centroid Cg3 of the five membered ring N3/C23-C24-C25-C26 of a 4-pypo-κO axial ligand of a nearby [Mg(TBrPP)(4-pypo-κO)$_2$] complex and the centroid Cg4 of the pyridyl ring N4/C29-C28-C27-C31-C32 of a 4-pypo-κO axial ligand of a neighboring [Mg(TBrPP)(4-pypo-κO)$_2$] molecule and vis verso. The Cg3…Cg4 distance is 3.998 (4) Å (Figure 9, Table S1).

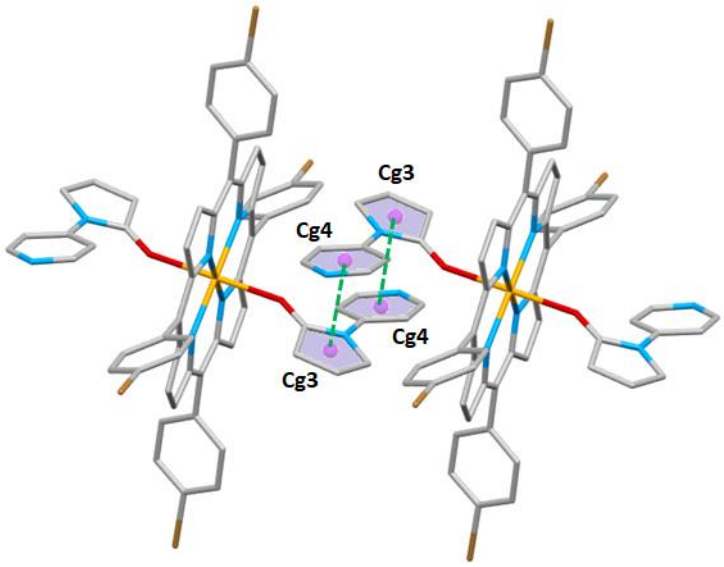

Figure 9. Drawing illustrating the Cg···Cg π intermolecular interactions in complex **1**.

The crystal packing of **1** is made by [Mg(TBrPP)(4-pypo-κO)$_2$] molecules parallel to the *a* axis which are linked by weak intermolecular interactions types C—H···N, C—H···O, C—H···Br and C—H···Cg as shown in Figure S6. The values of these intermolecular interactions are reported in Table S2.

3.5. Hirshfeld Surface Analysis

A Hirshfeld surface analysis on complex **1** was performed with the CrystalExplorer17.5 program **[35]** using standard surface resolution with the three-dimensional d_{norm} surfaces plotted over a fixed color scale of -0.0979 (red) to 1.7267 (blue) a.u. The three-dimensional d_{norm} surface of **1** is illustrated in Figure 10. In the two drawings of the latter figure, are shown the C31—H31···O1 distance between the carton C31 of one 4-pypo-κO axial ligand and the oxygen O1 of one 4-pypo-κO axial ligand of a neighboring [Mg(TBrPP)(4-pypo-κO)$_2$] and the C7—H7···Br1 non-conventional hydrogen bond between

the carbon C7 of pyrrole ring of one [Mg(TBrPP)(4-pypo-κO)$_2$] molecule and the bromine atom Br1 of a TBrPP porphyrinate of a nearby [Mg(TBrPP)(4-pypo-κO)$_2$] molecule.

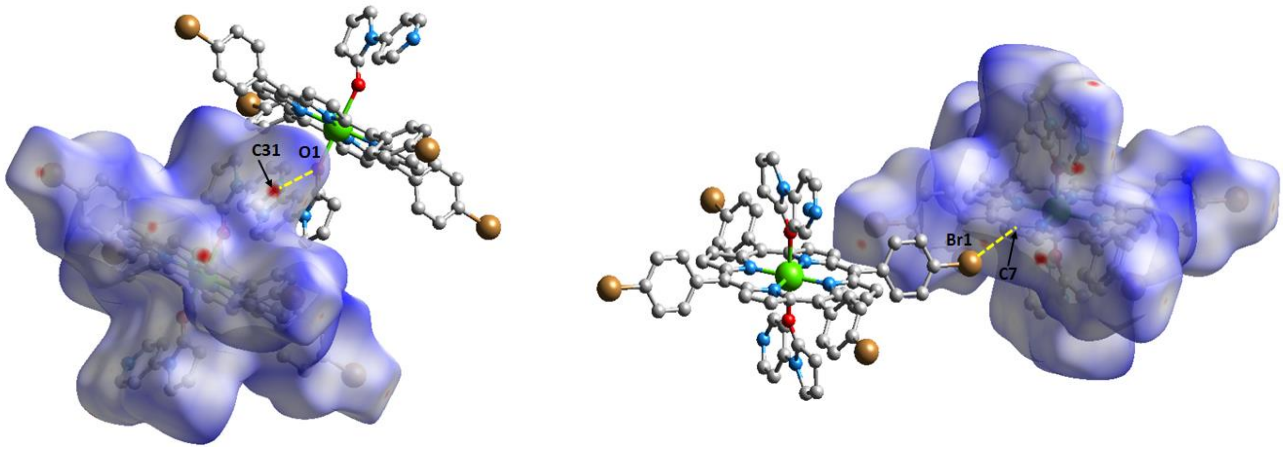

Figure 10. Hirshfeld surfaces of complex 1 mapped over d_{norm}.

The two-dimensional fingerprint plots are depicted in Table S7. The Hirshfeld surface analysis shows that in the crystal lattice of **1** are five major types of intermolecular non-conventional H bonds: H…H = 41.8%, Br…H = 22.6%, C…H = 21.1%, N…H = 5.1% and O…H = 2.2% on the d_{norm} surface.

The shape-index map of complex **1** (Figure 11-a) was generated in the range -1 to 1 Å. Concave red regions symbolize hydrogen-acceptor groups and convex blue regions symbolize hydrogen-donor groups interaction on the sharp-index map and are represented by adjacent red and blue triangles. This confirms the Cg···Cg π intermolecular interaction in the crystal lattice of **1** where Cg is the centroid of a five of six-member ring (Figure 9, Table S2). The curvedness map of the complex **1** (Figure 11-b) was generated in the range 4 to -4 Å. This curvedness plot shows flat surface patches characteristic of planar π-π stacking.

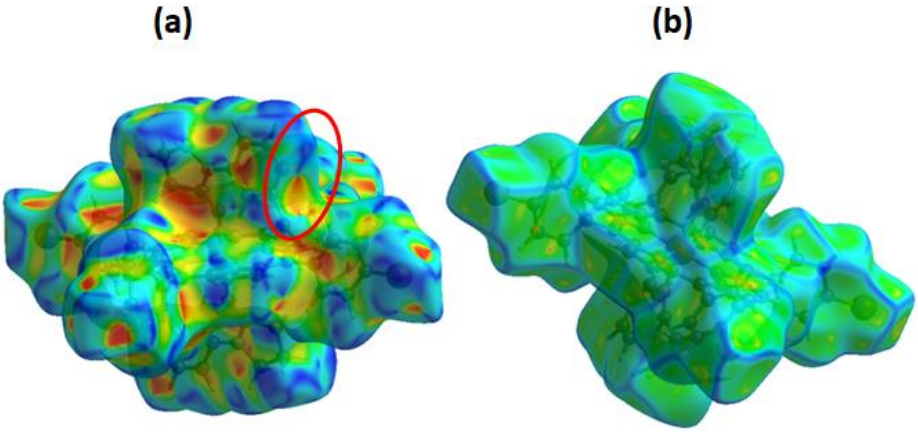

Figure 11. Shape Index surface **(a)** and curvedness surfaces **(b)** for complex **1**.

3.6. Cyclic voltammetry

Porphyrin complexes with non-electroactive divalent Mg(II) metal ion undergo three reversible one electron oxidations and one or two one electron reductions of the porphyrin core **[6]**. The cyclic voltammogram (CV) of complex **1**, shown in Figure 12, was recorded in dichloromethane using the tetra-*n*-butylammonium perchlorate (TBAP) as the supporting electrolyte (0.2 M). In the anode region of the CV, three one-electron oxidation waves are present. The first, second and third waves [O1/R1, O2/R2 and O3/R3] are reversible with half-potential values of 0.76, 0.92 and 1.42 V, respectively (Figure 12, Table 5). The cathodic region of the CV of **1**, shows only one reversible on-electron reduction wave with $E_{1/2}$ value of -1.50 V. All oxidations and reduction potential values of our TBrPP-Mg-(4-pypo-κO) species are very close to those of the Mg(II) metalloporphyrins reported in Table 5.

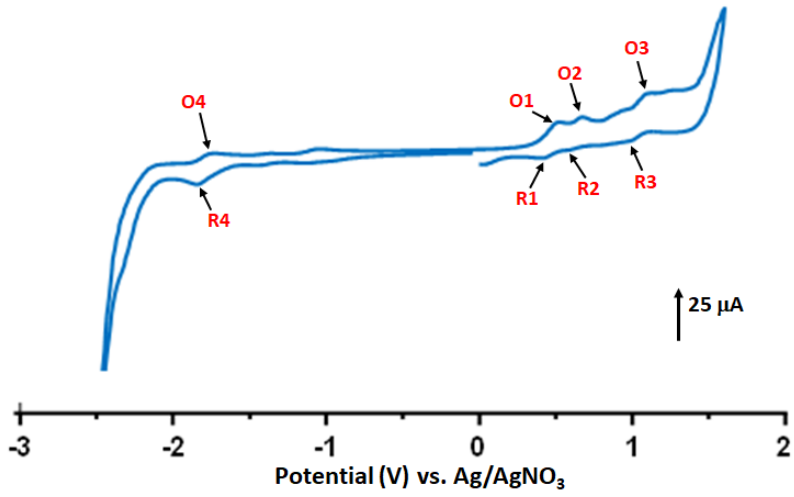

Figure 12. Cyclic voltammogram of [Mg(TBrPP)(4-pypo-κO)$_2$] (**1**). The solvent used is dichloromethane, and the concentration is ca. 10^{-3} M in 0.2 M TBAP, 50 mV/s, vitreous carbon working electrode (Ø= 3 mm).

As reported above, the (4-pypo-κO) - (4-pypo-κN) linkage isomerism is mainly related to the electron-withdrawing effect of the *para*-bromo groups of the TBrPP porphyrinate and the electron-donating effect of the *para*-methyl groups of the TPP porphyrinate. This phenomenon is reflected in the CV of [Mg(TBrPP)(4-pypo-κO)$_2$] (**1**) verses [Mg(TPP)(4-pypo-κN)$_2$]. Indeed, the (4-pypo-κO) isomer has higher oxidation potentials 0.76 V and 1.42 V compared to 0.62 V and 1.26 V of the (4-pypo-κO) isomer. Similarly [Mg(TBrPP)(4-pypo-κO)$_2$] (**1**) has a lower reduction potential of -1.5 V vs -1.62 V of [Mg(TPP)(4-pypo-κN)$_2$].

Table 5. Potentials (in V vs SCE) of the investigated complex **1** and a selection of related magnesium(II) *meso*-aryl-metalloporphyrins.

Compound	Oxidation			Reduction	Ref.
	1st Porph. Oxid. (O1,R1) ---------- $E_{1/2}$[a]	2st Porph. Oxid. (O2,R2) ---------- $E_{1/2}$[a]	3nd Porph. Oxid. (O3,R3) ---------- $E_{1/2}$[a]	1st Porph. Red. (R4,O4) ---------- $E_{1/2}$[a]	
[Mg(TClPP)(DMAP)][b,c]	0.63	0.91	1.22	–1.42	**[6]**
[Mg(TPP)(HMTA)$_2$][d,e]	0.73	0.99	-	–1.45	**[36]**
{[Mg(TPP)(pyz)]}$_n$[d,f]	0.65	0.95	-	–1.65	**[37]**
[Mg(TTP)(4-pypo-κN)$_2$][g]	0.62	1.04	1.26	-1.60	**[4]**
[Mg(TBrPP)(4-pypo-κO)$_2$] (**1**)	0.76	0.92	1.42	-1.50	t.w.

[a]: $E_{1/2}$ = half-wave potential, [b]: TClPP *meso*-tetrakis(*para*-chlorophenyl)porphyrinate, [c]: 4-dimethylaminopyridine, [d]: TPP = *meso*-tetraphenylporphyrinate, [e]: HTMA = hexamethylenetetramine, [f]: pyz = pyrazine, [g]: TTP = *meso*-tetra(*p*-tolyl)porphyrinate.

3.7. Theoretical study on the [Mg(TBrPP)(4-pypo-*κO*)$_2$] (1)

3.7.1. HOMO-LUMO iso-surfaces

Figure 13 shows the frontier molecular orbitals of complex **1** while in Table 6 are summarized several calculated reactivity parameters of **1** and the related [Mg(TTP)(DMAP)$_2$] coordination complex **[5]** taken as reference. The HOMO and LUMO iso-surfaces of **1** are localized in an equiprobably way around the center ion Mg(II). This demonstrates that the Mg^{2+} cation pulls electrons from the groups around it and fixes them close to it cyclically. The same interpretation is obtained for HOMO-1 and LUMO+1 molecular orbitals. The calculated energy required to move electrons from the π fundamental state (HOMO orbital) to the π* first excited state (LUMO orbital) known as the gap energy is 2.55 eV. This value which is very close to the experiment optical gap energy ($E_{g\text{-}opt}$ = 2.247 eV) indicates the semi-conductor character of our TBrPP-Mg-bis(4-pypo-*κO*) species (**1**). Therefore, **1** can be tested for sensor applications **[38,39]**.

According to the following relationship between the conductivity parameter and the gap energy : $\sigma \approx \exp\left(\frac{E_g}{k_B}\right).T$, where E_g is the gap energy and k_B is the Boltzmann constant, for [Mg(TBrPP)(4-pypo-*κO*)$_2$] (**1**) a value of 12.80 eV indicates that this coordination compound could be utilized as conductors **[40,41]**. The global reactive parameters are specified to identify the capacity of [Mg(TBrPP)(4-pypo-*κO*)$_2$] to accept or donate electrons. These parameters (Table 6) are very important to confirm the stability and the chemical reactivity of the studied species. The electrophilic index is calculated to be 2.99 eV indicating that this compound is an electrons-acceptor system. In addition, the chemical hardness (η) value of 1.28 eV is an indication that material is hard, which is also the case of the related Mg(II) complex [Mg(TTP)(DMAP)$_2$] species **[5]** (Table 6). The negative value of the chemical potential (μ = -3.77 eV) indicates that this compound is stable. This value is quite higher than that of [Mg(TTP)(DMAP)$_2$] (μ = -2.831 eV). Therefore, according to the values of the parameters depicted in Table 6, one can conclude that complex **1** is reactive, stable, and a hard system.

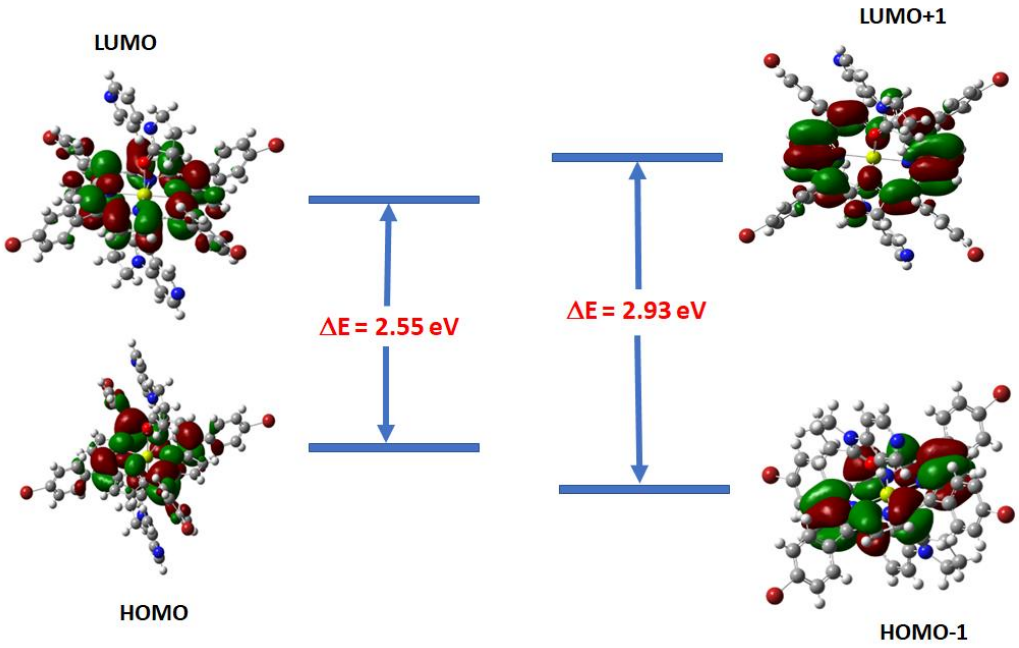

Figure 13. HOMO-LUMO and HOMO-1 – LUMO+1 plots of complex **1**.

Table 6. TD-DFT calculations of complex **1** and [Mg(TTP)(DMAP)$_2$] **[5]** at the B3LYP/LanL2DZ level of theory (in dichloromethane solvent) of HOMO-LUMO energy gap, chemical potential, electronegativity, global hardness, global softness, and electrophilicity index.

Function	Values	
	Complex **1**	[Mg(TTP)(DMAP)$_2$] **[5]**
E_{HOMO} (eV)	-5.04	-4.108
E_{LUMO} (eV)	-2.49	-1.555
E_{LUMO}-E_{HOMO} = *Gap energy* (eV)[a]	2.55	2.553
Ionisation potential (eV)[b]	5.05	~-4.108
Electron affinity (eV)[c]	-2.49	~-1.555
Chemical potential μ (eV)[d]	-3.77	-2.831
Mulliken electronegativity χ [e]	3.77	-
Global hardness η (eV)[f]	1.28	1.276
Global Softness S (eV)[g]	0.39	-
Global electrophilicity index ψ (eV)[i]	2.99	-

a: *Gap energy* = E_{LUMO}-E_{HOMO}, b: *Ionisation potential* ≈ -E_{LUMO}, c: *Electron affinity* ≈ -E_{LUMO}, d: *Chemical potential* $\mu = 1/2(E_{LUMO} + E_{LUMO})$, e: *Mulliken electronegativity* = χ = - μ, f: *Global hardness* $\eta = 1/2(E_{LUMO} - E_{LUMO})$, *g Global Softness S* = $1/2\eta$, i: *Global electrophilicity index* $\psi = \mu^2 l 2\eta$.

3.7.2. MEP and optimized structure of [Mg(TBrPP)(4-pypo-κO)$_2$] (1)

The geometry of complex **1** is optimized at the DFT-D3/B3LYP/GENECP level of theory **[42-44]**. based on the Cif file obtained from the X-ray diffraction analysis of **1**. The H, C, N, O, Br, and the Mg center metal are optimized at 6-311G(d, p), LanL2DZ **[45]**, and 6-311G(d, p) **[47]**, respectively. The 3D molecular system was visualized by the Vesta package **[47]**. The calculated stable structure is shown in Figure 14. The calculated Mg—O(4-pypo-κO) distance is 2.22 Å which is very close to the experiment distance value of 2.223(4) Å and the theoretical C=O bond length of the (4-pypo-κO) ligand in **1** is 1.22 Å which is also very close to the experiment value of 1.224(6) Å.
The molecular electrostatic potential (MEP) calculations are very useful to identify the electrophilic and nucleophilic sites in the studied compound and recently, it has appeared important to predict the desired binding in a biological identification **[41]**.

From 3D-MEP, three regions are obtained where the first is for a negative potential (electron-rich zone), the second is specified for a negative potential (electron-poor zone), and the third has a zero potential (neutral zone). From the MEP plots, it is demonstrated that our studied compound is characterized as electrophilic. As a result, complex **1** can be used in sensor applications. It appears to be a small red spot between the (4-pypo-κO) axial ligand and the magnesium center metal. The blue color in a MEP map refers to the potential positive ($V(r) < 0$: electron-poor zone), the red is used for potential negative values ($V(r) > 0$: electron-rich zone) while the green color indicates ($V = 0$) a zero potential. Okulik *et al.,* **[48]** reported that the blue arias indicate an electrophilic reactivity while the red color illustrates the strongest repulsion in the MEP map. The MEP map for **1** is depicted in Figure 15 where the color code is between $-4.0.10^{-6}$ u.a (red color) and $4.0.10^{-6}$ u.a. (blue color). The red-colored regions are located around the N atom of the benzene group of ligands. The blue color is shown in the two (4-pypo-κO) axial ligands indicating that [Mg(TBrPP)(4-pypo-κO)$_2$] (**1**) presents an electrophilic aspect in these regions.

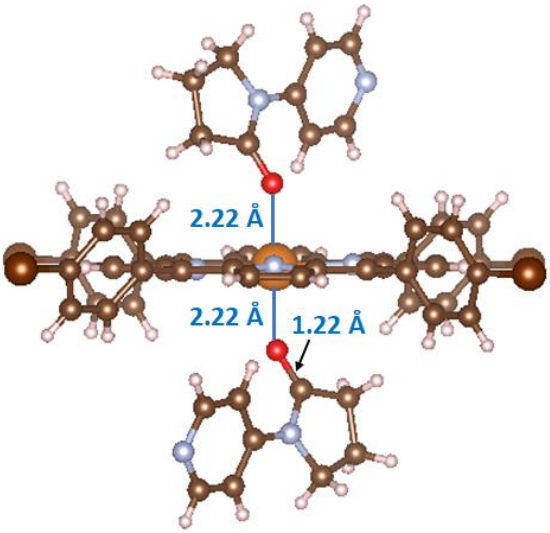

Figure 14. Optimized structure of complex 1.

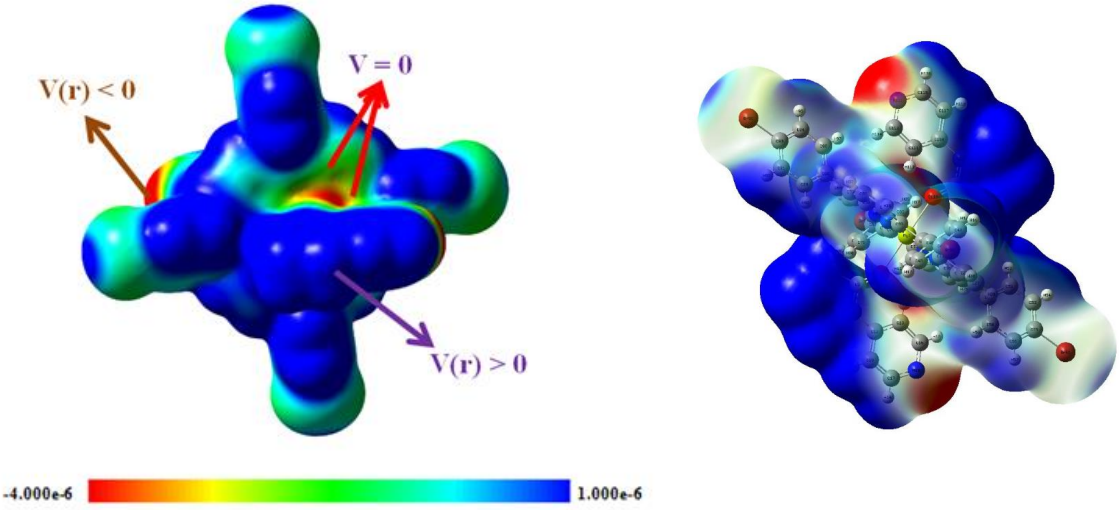

Figure 15. MEP iso-surface of complex **1**.

3.7.3. QTAIM and NCI-RDG analyses

Since the electronic and the geometrical parameters may not be enough to explain clearly the intermolecular interactions between the two (4-pypo-*κO*) axial ligands and the [Mg(TBrPP)] moiety we have studied the electronic density parameters of our complex using the quantum theory of atom in molecule (QTAIM) **[49-51]**. The deficiency of the electronic charges in the interatomic path was

identified by using the Non-Covalent Interactions (NCI) index **[52,53]**. The NCI-RDG analysis was performed in order to get a visual representation of weak interactions within a system. The Multiwfn program **[54]** was used to execute the QTAIM topological parameters using the bond critical points (BCPs) in our compound from the wfn file generated from the chk file of the Gaussian 09 package **[55]**. This powerful approach encompasses all the types of interactions that can be formed between the [Mg(TBrPP)] moiety and the two axial ligands. The QTAIM theory can be used to calculate the electron density ($\rho(r)$), Laplacian of electron density ($\nabla^2\rho(r)$), kinetic energy density (G(r)), potential energy density (V(r)) and total electron energy density (H(r)), the ellipticity of electron density $\varepsilon(r)$ in the bonding characteristics and the estimated interaction energy (E_{int}) of two atoms. Figure 16 depicts the AIM molecular graphs while the topological parameters are shown in Table 7 of complex **1**. The selected Bond Critical Points (BCPs) between the [Mg(TBrPP)] moiety and the two axial ligands (4-pypo-κO) of complex **1** have been determined using QTAIM analysis. As shown in Figure 16 and Table 7, these three moieties, form eight interactions (BCP_1 – BCP_8) among them BCP_1 and BCP_2 correspond to the interactions of the Mg(II) center ion and the oxygen atoms O1 and O1i (the centrosymmetric oxygen atom) of the two *trans* axial ligands (4-pypo-κO) of **1**. In Table 7, it is shown that the [Mg(TBrPP)(4-pypo-κO)$_2$] complex **1** has a positive value for the Laplacian, indicating the presence of non-covalent interactions. The electronic density ($\rho(r)$) values range from 0.0039 to 0.0206 a.u. The Laplacian of electron density $\nabla^2\rho(r)$ varies from 0.0025 to 0.1537 a.u. It is demonstrated a week electrostatic interaction between [Mg(TBrPP)] and the 4-pypo-κO axial ligand (Figure 17). This result is explained by the fact that $\nabla^2\rho(r) > 0$ and $H(r) > 0$. In $BCP_{1\text{-}2}$, low values of H(r) indicate that the two (4-pypo-κO) ligands are stabilized by coordination bond type with the Mg(II) center metal. This result is confirmed by the appearance of a green spot between the two oxygen atoms O1 and $O1^i$ ($O1^i$ = symmetry related O1) of the two trans (4-pypo-κO) axial ligands and the Mg center metal (Figure 17). In addition, the two (4-pypo-κO) axial ligands are symmetrically stabilized by forming four van der Waals bonds with the N and C atoms of [Mg(TBrPP)(4-pypo-κO)$_2$] (**1**) ($BCP_{3,4}$ and $BCP_{5,6}$) which confirms the experimental results obtained by X-ray diffraction (see crystallographic section) . This information is explained by the appearance of green spots in the NCI index (Figure 17-a). These interactions are found to be less stable than O-Mg interactions. In the RDG iso-surface, there is a wide band located between -0.015 and 0.015 a.u. (Figure 17-b). Furthermore, the two (4-pypo-κO) ligands form weak interactions

between several hydrogen atoms of these moieties and the carbon atoms of the phenyls in the *para*-positions of TBrPP porphyrinate.

The calculated interaction energy ($E_{int.}$) is determined by the equation of Espinosa *et al.* ($E_{int.}$= V(r)/2) **[56].** From Table 7, it is found that the high interaction energy is located on BCP_1, BCP_2, BCP_4, and BCP_5. The $E_{int.}$ values range from -10.5 kJ.mol^{-1} to -13.12 kJ.mol^{-1}. It is concluded that the two O···Mg interactions are responsible for the stability of complex **1**.

Table 7. The topological parameters calculated at selected bond critical points BCPs (All parameters are given in a.u., except E_{int} is expressed in kJ.mol^{-1}) of complex **1**.

BCP	**ρ(r)**	**$\nabla^2\rho(r)$**	**G(r)**	**V(r)**	**ε(r)**	**H(r)**	**$E_{int.}$**
BCP_1	0.0205	0.1535	0.0111	-0.0109	0.02	0.0001	**-13.12**
BCP_2	0.0206	0.1537	0.0111	-0.0109	0.02	0.0001	**-13.12**
BCP_3	0.0132	0.0396	0.0092	-0.0091	0.70	0.0001	**-10.50**
BCP_4	0.0143	0.0578	0.0123	-0.0101	0.28	0.0021	**-5.251**
BCP_5	0.0132	0.0397	0.0092	-0.0091	0.69	0.0001	**-10.50**
BCP_6	0.0143	0.0578	0.0123	-0.0101	0.28	0.0021	**-5.25**
BCP_7	0.0039	0.0131	0.0025	-0.0018	0.82	0.0007	**-0.26**
BCP_8	0.0039	0.0131	0.0025	-0.0018	0.82	0.0007	**-0.26**

ρ(r) = electron density, $\nabla^2\rho(r)$ = Laplacian of electron density, G(r) = kinetic energy density, V(r) = potential energy density, Δρ(r) = the deformation density, H(r) = the energy density H(r), and E_{int} = the estimated interaction energy (E_{int}, in kJ.mol^{-1}).

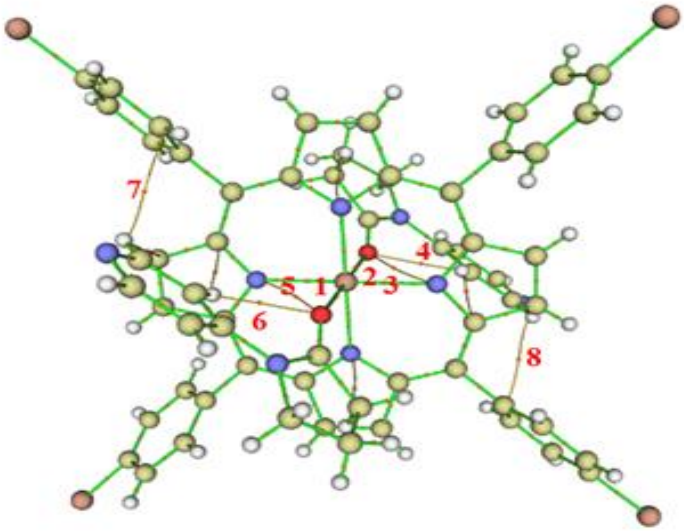

Figure 16. AIM analyses of complex **1**. Bond critical points (BCPs) are represented with small red spheres.

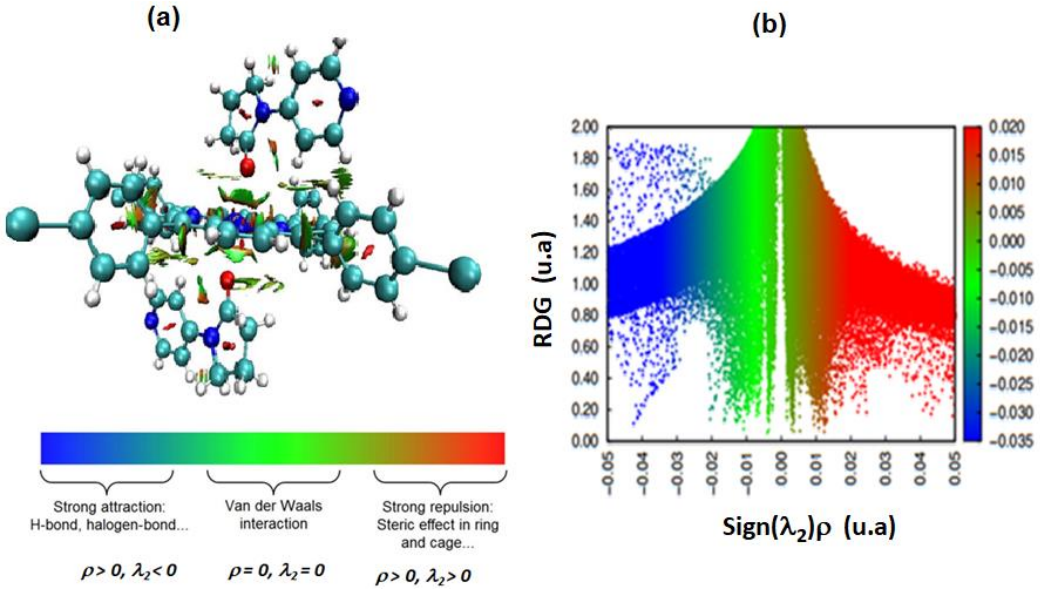

Figure 17. **(a):** RDG function iso-surface with sign(λ_2) $\rho(r)$ coloring scheme complex **1**, **(b):** Reduced Density Gradient analysis (RDG) iso-surface**.** with λ_2 is the second Hessian eigenvalue and sign(λ_2) is the second largest eigenvalue of the electron density Hessian matrix.

4. Conclusion

In summary, synthesis, spectroscopic and cycle voltammetry characterizations of the *O*-coordinated 4-pyrrolidinopyridine axial ligand (4-pypo-*κO*) magnesium(II) porphyrin complex [Mg(TBrPP)(4-pypo-*κO*)$_2$] (**1**) is reported. The structural analysis by single crystal X-ray diffraction was elucidated. Notably, the photophysical properties of complex **1** and those of the *N*-coordinated 4-pyrrolidinopyridine axial ligand (4-pypo-*κN*) [Mg(TTP)(4-pypo-*κN*)$_2$] linking isomer are almost identical and in the solid state both isomers exhibit parallel (4-pypo-*κN*) and (4-pypo-*κO*) axial ligands. In this paper, DFT, MEP and QTAIM methods were employed to investigate the various features of complex **1**. Thus, the DFT/TDDFT calculations show that complex **1** is reactive, stable, and a hard system while the 3D-MEP ab initio calculations indicate that our TBrPP-Mg(II)-(4-pypo-*κN*) species presents electrophilic properties. Finally, the QTAIM method indicates that the interaction between the [Mg(TBrPP)] moiety and the (4-pypo-*κO*) axial ligand is as expected a coordination bond between the Mg(II) center metal and the oxygen atom of the 4-pyrrolidinopyridine ligand.

Declaration of Competing Interest

The authors declare that they have no known competing financial interests or personal relationships that could have appeared to influence the work reported in this paper.

Supporting information

CCDC-2220695 contain the supplementary crystallographic data of complex **1**. These data can be obtained free of charge from the Cambridge Crystallographic Data Centre via www.ccdc.cam.ac.uk/data_request/cif.

Acknowledgements

The authors gratefully acknowledge to the deanship of the Scientific Research at Majmaah University, Saudi Arabia.

4. References

[1] J.W. Buchler, "The porphyrins", Vo. 1, Part A, D. Dolphin Ed. pp. 390-474, Academic Press, New York, (1978)].

[2] N. Amiri, F. Ben Taheur, S. Chevreux, E. Wenger, G. Lemercier, H. Nasri, Tetrahedron 73 (2017) 7011-7016, https://doi.org/10.1016/j.tet.2017.10.029.

[3] K. Ezzayani, Z. Denden, S. Najmudin, C. Bonifácio, E. Saint-Aman, F. Loiseau, H. Nasri, Eur. J. Inorg. Chem. 2014, 5348–5361 doi:10.1002/ejic.201402546.

[4] S. Jabli, S. Hrichi , R. Chaabane-Banaoues, F. Molton , F. Loiseau, T. Roisnel, I. Turowska-Tyrk, H. Babba, H. Nasri, J. Mol. Struct. 1261 (2022) 132882, https://doi.org/10.1016/j.molstruc.2022.132882.

[5] S. Jabli, M. Chaabene, T. Roisnel, F. Molton, F. Loiseau, P. Jehan, R. Ben Chaabane, H. Nasri, , J. Mol. Struct. 1267 (2022) 133559, https://doi.org/10.1016/j.molstruc.2022.133559.

[6] T. Fradi, O. Noureddine, F. Ben Taheur, M. Guergueb, S. Nasri, N. Amiri, A. Almahri, T. Roisnel, V. Guerineau, N. Issoui, H. Nasri, J. Mol. Struct.1236 (2021) 130299, hnasri1@gmail.com , habib.nasri@fsm.rnu.tn

[7] Z. Denden, K. Ezzayani, E. Saint-Aman, F. Loiseau, S. Najmudin, C. Bonifácio, J.-C. Daran, H. Nasri, Eur. J. Inorg. Chem. 2015, 2596–2610, doi:10.1002/ejic.201403214.

[8] J.D Petke, G.M Maggiora, L.L Shipman, R.E Christoffersen, J. Mol. Spectrosc. 71 (1978) 64-84, https://doi.org/10.1016/0022-2852(78)90075-9.

[9] Q. Wang, C.-H. Guo, J. Jia, H.-S. Wu, 179 (2015). J Mol Model 21,179 (2015). https://doi.org/10.1007/s00894-015-2733-y.

[10] C. Maeda, J. Shimonishi, R. Miyazaki, J.-Y. Hasegawa, T. Ema, Chem. Eur. J. 22 (2016) 6556–6563, doi:10.1002/chem.201600164.

[11] P. Yan, J. Cao, J. Pang, Zi. Yang, X. Wang, X. Yao, Org. Electron. 93 (2021) 106158, https://doi.org/10.1016/j.orgel.2021.106158.

[12] J. Kesters, P. Verstappen, M. Kelchtermans, L. Lutsen, D. Vanderzande, W. Maes, Adv. Energy Mater. 5 (2015) 1500218, https://doi.org/10.1002/aenm.201500218.

[13] A.D.F. Dunbar, S. Brittle, T.H. Richardson, J. Hutchinson, C.A. Hunter, J. Phys. Chem. B 114 (2010) 11697–11702, https://doi.org/10.1021/jp102755h.

[14] M. Biesaga, K. Pyrzyńska, M. Trojanowicz, Talanta 51 (2000) 209-224, https://doi.org/10.1016/S0039-9140(99)00291-X.

[15] R. Das, T. Ezhil, A.S. Palakkal, D. Muthukumar, R.S. Pillai, C.M. Nagaraja, J. Mater. Chem. A, 9 (2021) 23127-23139, https://doi.org/10.1039/D1TA05138E.

[16] A.O. Atoyebi, C. Brückner, Inorg. Chem. 58 (2019) 9631–9642, https://doi.org/10.1021/acs.inorgchem.9b00052.

[17] C.R. Groom, I.J. Bruno, M.P. Lightfoot, S.C. Ward, Acta Cryst. B72 (2016) 171–179, https://doi.org/10.1107/S2052520616003954

[18] C.C. Ong, V. McKee, G.A. Rodley, Inorg. Chim. Acta 123 (1986) L11–L14, doi: 10.1016/S0020-1693(00)84300-5.

[19] N. Amiri, S. Nasri, T. Roisnel, G. Simonneaux, H. Nasri, Acta Crystallogr., Sect.E:Cryst. Commun. 17 (2015) m73-m74, https://doi.org/10.1107/S2056989015003722.

[20] E.J. Shin, D. Kim, J. Photochem. Photobiol. A152 (2002) 25–31, doi: 10.1016/S1010-6030(02)00189-2.

[21] A.D. Adler, F.R. Longo, J.D. Finarelli, J. Goldmacher, J. Assour, L. Korsakoff, J. Org. Chem. 32 (1967) 476–476, https://doi.org/10.1021/jo01288a053.

[22] R. Timkovich, A. Tulinsky, J. Am. Chem. Soc. 91 (1969) 4430–4432. https://doi.org/10.1021/ja01044a018.

[23] Bruker (2004). SAINT, APEX2 and SADABS. Bruker AXS Inc., Madison, Wisconsin, USA.

[24] Burla, M. C., Caliandro, R., Carrozzini, B., Cascarano, G. L., Cuocci, C., Giacovazzo, C., Mallamo, M., Mazzone, A. & Polidori, G. (2015). J. Appl. Cryst. 48, 306–309., https://doi.org/10.1107/S1600576715001132.

[25] G. M. Sheldrick, Acta Cryst , C71 (2015) 3., https://journals.iucr.org/c/issues/2015/01/00/index.html

[26] Farrugia, L. J. (2012). J. Appl. Cryst. 45, 849–854. https://doi.org/10.1107/S0021889812029111.

[27] C.F. Macrae, I.J. Bruno, J.A. Chisholm, P.R. Edgington, P. Mc Cabe, E. Pidcock, L. Rodriguez-Monge, R. Taylor, J. van de Streek, P.A. Wood, J Appl Crystallogr. 41 (2008) 466–470. https://doi.org/10.1107/S0021889807067908.

[28] H. Ogoshi, N. Masai, Z. Yoshida, J. Takemoto, K. Nakamoto, Bull. Chem. Soc. Jpn. 44 (1971) 49–51., https://doi.org/10.1246/bcsj.44.49.

[29] K. Colladet, M. Nicolas, L. Goris, L. Lutsen, D. Vanderzande, Thin Solid Films 451 (2004) 7–11, doi: 10.1016/j.tsf.2003.10.085.

[30] C.C. Ong, V. McKee, G.A. Rodley, Inorg. Chim. Acta 123 (1986) L11–L14, doi: 10.1016/S0020-1693(00)84300-5.

[31] N. Amiri, F. Ben Taheur, S. Chevreux, C.M. Rodrigues, V. Dorcet, G. Lemercier, H. Nasri, Inorg. Chim. Acta 525 (2021) 120466, https://doi.org/10.1016/j.ica.2021.120466.

[32] V. McKee, O.C. Choon, G.A. Rodley, Inorg. Chem. 23 (1984) 4242–4248, doi: 10.1021/ic00193a029.

[33] M.P. Byrn, C.J. Curtis, Y. Hsiou, S.I. Khan, P.A. Sawin, S.K. Tendick, A. Terzis, C.E. Strouse, J. Am. Chem. Soc. 115 (1993) 9480–9497, doi: 10.1021/ja0 0 074a013.

[34] K. Ezzayani, S. Nasri, M. S. Belkhiria, J.-C. Daran, H. Nasri, Acta Crystallogr., Sect.E: Struct. Rep. Online (2013), 69, m114, https://doi.org/10.1107/S1600536813001219.

[35] Turner, M.J.; McKinnon, J.J.; Wolff, S.K.; Grimwood, D.J.; Spackman, P.R.; Jayatilaka, D.; Spackman, M.A. CrystalExplorer17; The University of Western Australia : Perth, Australia, 2017.

[36] K. Ezzayani, A. Ben Khelifa, E. Saint-Aman, F. Loiseau, H. Nasri, Journal of Molecular Structure 1137 (2017) 412-418, http://dx.doi.org/10.1016/j.molstruc.2017.02.054

[37] A.B. Khelifa, K. Ezzayani, M. Guergueb, F. Loiseau, E. Saint-Aman, H. Nasri, J. Mol. Struct. (2020) 129508, doi: 10.1016/j.molstruc.2020.129508.

[38] R. Soury, M. Chaabene, M. Jabli, T.A. Saleh, R. Ben Chaabane, E. Saint-Aman, F. Loiseau, C. Philouze, A.-R. Allouche, H. Nasri, J. Chem. Eng. 375 (2019) 122005. https://doi.org/10.1016/j.cej.2019.122005.

[39] S. Arshadi, F. Abdolahzadeh, E. Vessally, J. Mol. Graph. Model. (2022) 108371. https://doi.org/10.1016/j.jmgm.2022.108371.

[40] Z. Pu, B. Xiao, S. Mao, Y. Sun, D. Ma, H. Wang, J. Zhou, Y. Cheng, J.-W. Shi, J. Colloid Interface Sci.. 628 (2022) 477–487. https://doi.org/10.1016/j.jcis.2022.08.080.

[41] A. Kechich, R. Soury, M. Jabli, K.M Alenezi, C. Philouze, H. Nasri, Inorganic Chemistry Communications 128 (2021) 108588, https://doi.org/10.1016/j.inoche.2021.108588.

[42] S. Grimme, J. Chem. Phys. 124 (2006), https://doi.org/10.1063/1.2148954 034108.

[43] S. Grimme, J. Antony, S. Ehrlich, H. Krieg, J. Chem. Phys. 132 (2010), https://doi.org/10.1063/1.3382344154104.

[44] C. Lee, W. Yang, R.G. Parr, Phys. Rev. B. 37 (1988) 785–789, https://doi.org/10.1103/PhysRevB.37.785.

[45] P.J. Hay, W.R. Wadt, J. Chem. Phys. 82 (1985) 270–283, https://doi.org/10.1063/1.448799.

[46] A.A. Aboalhassan, S.A. El-Daly, E.-Z. M. Ebeid, M.A.S. Sakr, J. Photoch. Photobio. A. 431 (2022) 114039. https://doi.org/10.1016/j.jphotochem.2022.114039.

[47] VESTA, (n.d.). https://jp-minerals.org/vesta/en/

[48] N. Okulik, A. H. Jubert, Internet Electron. J. Mol. Des. 4 (2005) 17–30, http://www.biochempress.com.

[49] C. Mchiri, B. Gassoumi, S. Acherar, M.A.M. Sh. El-Sharief, H. Nasri, Inorganic Chemistry Communications. 133 (2021) 108924., https://doi.org/10.1016/j.inoche.2021.108924.

[50] R. F. W. Bader, Atoms in Molecules: A Quantum Theory, Oxford University Press, Oxford, New York, 1994.

[51] P.S.V. Kumar, V. Raghavendra, V. Subramanian, J Chem Sci. 128 (2016) 1527–1536. https://doi.org/10.1007/s12039-016-1172-3.

[52] H. Raissi, M. Yoosefian, A. Hajizadeh, J. shakhs Imampour, M. Karimi, F. Farzad, Bull. Chem. Soc. Jpn. 85 (2012) 87–92. https://doi.org/10.1246/bcsj.20110177.

[53] H. Raissi, F. Farzad, E.S. Nadim, M. Yoosefian, H. Farsi, A. Nowroozi, D. Loghmaninejad, Int. J. Quantum Chem. 112 (2012) 1273–1284, https://doi.org/10.1002/qua.23123.

[54] T. Lu, F. Chen, J. Comput. Chem. 33 (2012) 580–592, https://doi.org/10.1002/jcc.22885.

[55] G09 Gaussian.com, http://gaussian.com/glossary/g09/.

[56] E. Espinosa, C. Lecomte, E. Molins, Chem. Phys. Lett. 300 (1999) 745–748, https://doi.org/10.1016/S0009-2614(98)01399-2.

We report the synthesis of the [Mg(TBrPP)(4-pypo-κO)$_2$] (**1**) complex where TBrPP is the *meso*-tetra(*para*-bromophenyl)porphyrinate and 4-pypo-κO is the *O*-bonded 4-pyrrolidinopyridine axial ligand. This Mg(II) coordination is considered the linking isomer of the already known *N*-bonded 4-pyrrolidinopyridine (4-pypo-κN) with the formula [Mg(TTP)(4-pypo-κN)$_2$] where TTP is the *meso*-tetra(*p*-tolyl)porphyrinate. Complex **1** was characterized by elemental analysis, IR, ^{1}H NMR, UV/Vis and fluorescence spectrometric techniques, cyclic voltammetry measurements as well as single-crystal X-ray diffraction analysis.

Computational studies were used to elucidate the minimum energy geometry, the HOMO – LUMO molecular orbitals characteristics and the reactivity of complex **1**. The molecular electrostatic potential (MEP) calculations on complex **1** have been made to determine the electrophilic-nucleophilic character of our new Mg(II) metalloporphyrin. Furthermore, the quantum theory atom in molecule (QTAIM) calculations were performed to get more insights into the type of interactions between the [Mg(TBrPP)] moiety and the two 4-pyrrolidinopyridine axial ligand of complex **1**.

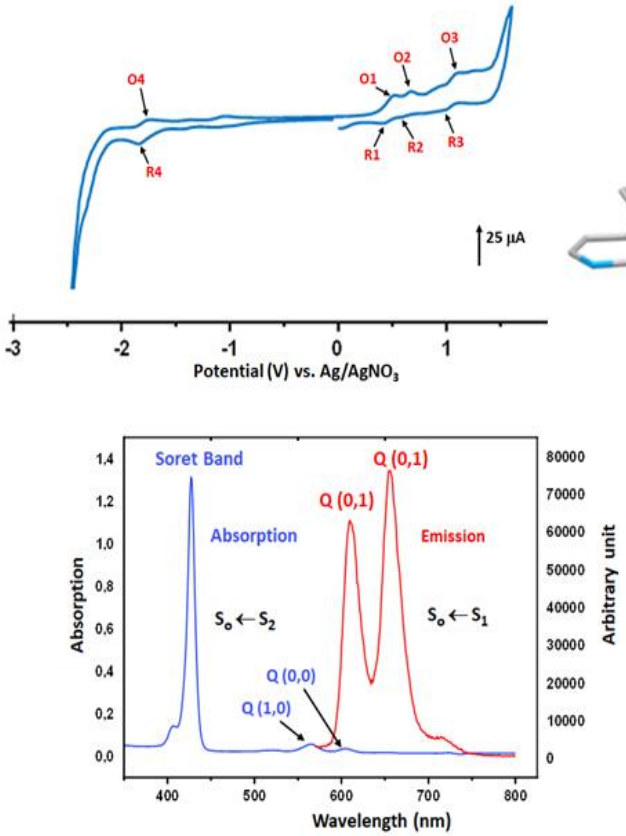

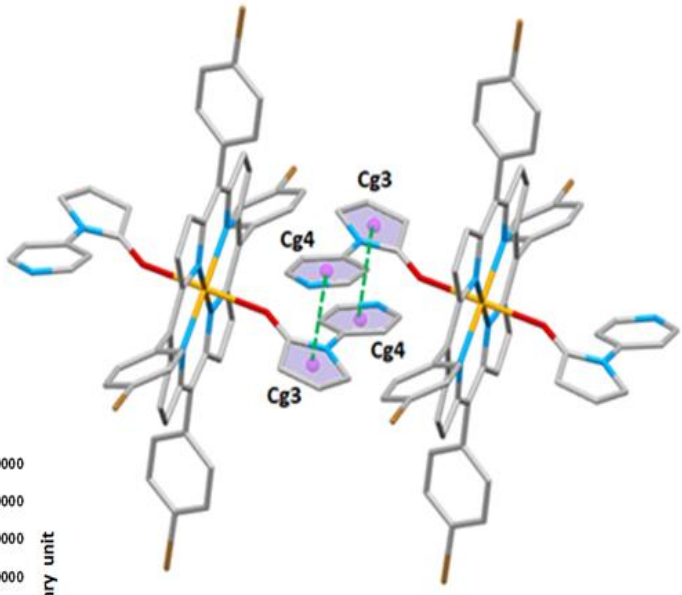

Credit author statment

Habib Nasri and H. Ghalla performed written – original draft, , performed writing – review and editing, Souhir Jabli, Soumaya Nasri, Emiliano Martinez Vollbert, Florian Molton and Thierry Roisnel, Bouzide Gassoumi performed Formal analysis, Frédérique Loiseau performed Conceptualization – Resources.

Declaration of Competing Interest

The authors declare that they have no known competing financial interests or personal relationships that could have appeared to influence the work reported in this paper.